

ATLAS Internal Note  
CAL-NO-062  
Date

## Study of Optimum Integration Times for the ATLAS Hadronic End-Cap Calorimeter

A. Kiryunin  
Institute for High Energy Physics,  
Protvino, 142284 Moscow region, Russia

M. Lefebvre  
University of Victoria, Physics and Astronomy,  
Victoria, British Columbia, Canada V8W 3P6  
(Visitor at the Laboratoire de l'Accélérateur Linéaire,  
bât. 200, 91405 Orsay, France)

C.J. Oram and W. Roberts  
TRIUMF, 4004 Wesbrook Mall,  
Vancouver, British Columbia, Canada V6T 2A3

H. Brettel and H. Oberlack  
Max-Planck-Institut für Physik,  
Föhringer Ring 6, D-80805 München, Germany

### Abstract

Assuming a luminosity of  $1.0 \times 10^{34} \text{ cm}^{-2}\text{s}^{-1}$  and an inelastic cross section of 70 mb, minimum bias events were generated with PYTHIA in the ATLAS end-cap calorimeter region. From an analysis of these events along with readout and electronic noise calculation, optimum integration times for the ATLAS hadronic end-cap readout channels have been obtained. In light of these optimum values a set of four  $t_p(\delta)$  have been chosen for the shaper, namely 20, 30, 40 and 50 ns, and each readout channel assigned a suitable shaper. Values of the calculated noise for each readout channel using its assigned preamplifier are presented.

# 1 Introduction

In this note we present the results of a study of the optimum shaping times  $t_p(\delta)$  for the end-cap hadronic calorimeter readout channels in the case of minimum ionising particles.

For each readout channel, the electronic noise (section 2) and the pileup noise (section 3) are obtained as a function of  $t_p(\delta)$ . The corresponding optimum  $t_p(\delta)$  is then calculated by minimising the total noise (section 4).

## 2 Electronic Noise

The amplifiers have been parametrised in PSPICE [1]. However a separate PSPICE for every channel of the calorimeter for various shaping times was considered impractical for the purposes of this study. Hence the electronic readout signal and noise were calculated following ref. [2]. These calculations were compared to PSPICE simulations for a representative set of 27 values of detector capacitances  $C_d$  and transmission line lengths  $t_l$ . An rms difference of 12% in the noise values obtained was found. All calculations assumed the mechanical structure of the of the end-cap calorimeter [3].

For signal shaping, a CR2RC2 (bipolar) filter was used assuming a charge preamplifier. In the calculation, this is equivalent to a CRRC3 (unipolar) filter for a current preamplifier. Series noise, parallel noise and lossy line noise were computed. The lossy transmission line modelled has a propagation delay of 5 ns/m, a  $R_o = 50 \Omega$  characteristic impedance and a skin effect resistance of 1.5  $\Omega$ /m at 10 MHz and 300 K. The second stage noise (including the summing logic noise) is neglected in this study. We also define the following peaking times:

- $t_p(\delta)$  peaking time (5 to 100%) of the preamplifier and filter only for a delta pulse;
- $t_m(\delta)$  peaking time (5 to 100%) of the output signal for delta pulse;
- $t_m(\Delta)$  peaking time (5 to 100%) of the output signal for a triangle pulse;

The pure delay caused by the transmission line is not included in this analysis, but delays caused by the signal distortion due to losses in the transmission line are treated. Note that  $t_p(\delta)$  and  $t_m(\delta)$  coincide in the limit of vanishing detector capacitance  $C_d$  and transmission line length  $t_l$ .

Figures 1 and 2 show the output signal curves corresponding to various  $t_p(\delta)$  for delta and triangle input signal respectively, for the case of a detector capacitance of  $C_d = 124.9$  pF and a transmission line length  $t_l = 6.43$  ns. The corresponding peaking times  $t_p(\delta)$ ,  $t_m(\delta)$  and  $t_m(\Delta)$  are shown, along with the filter time constant  $\tau$  (only  $t_p(\delta)$  and  $\tau$  do not depend on  $C_d$  and  $t_l$ ). The drift time assumed is 350 ns.

The electronic noise computed for the same value of the detector capacitance  $C_d$  is shown in figure 3 as a function of the transmission line length  $t_l$  for two triangle peaking times. Though the transmission line is in liquid argon (LAr) in the end-cap hadronic calorimeter, the noise is also shown at room temperature for comparison.

Each readout channel is made up of a number of preamplifiers in the LAr. Each preamplifier is in general connected to one tile, but up to 4 tiles can be ganged in parallel to one preamplifier. Table 1 shows for each readout channel the number of preamplifiers

and the number of tiles. This proposed ganging scenario is still under study. Per end-cap, for each readout segmentation in phi, there is a total of 740 preamplifiers distributed in 69 readout channels.

The noise associated with each preamplifier must be calculated to form the total electronic noise in a readout channel. To this end, the detector capacitance and the transmission line length associated with each preamplifier are needed. They have been calculated taking into account the proposed geometry for the end-cap hadronic calorimeter, the proposed transmission line routing to the preamplifier boards, and the proposed partial tile ganging. The resulting detector capacitances vary between 7 pF and 270 pF and are shown in figure 4. Transmission line lengths vary between 365 mm and 2170 mm and are shown in figure 5.

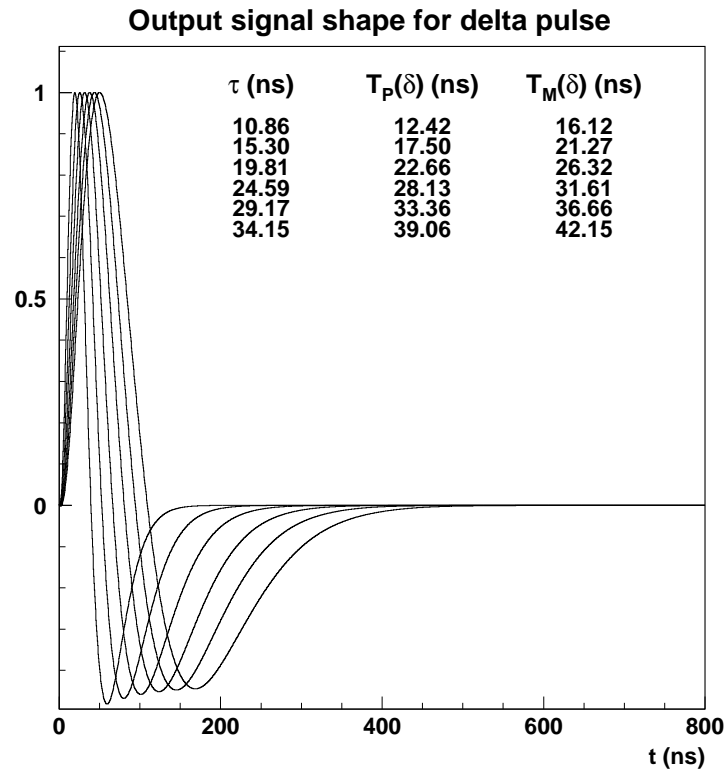


Figure 1: Example of output signal curves for delta pulses (see text).

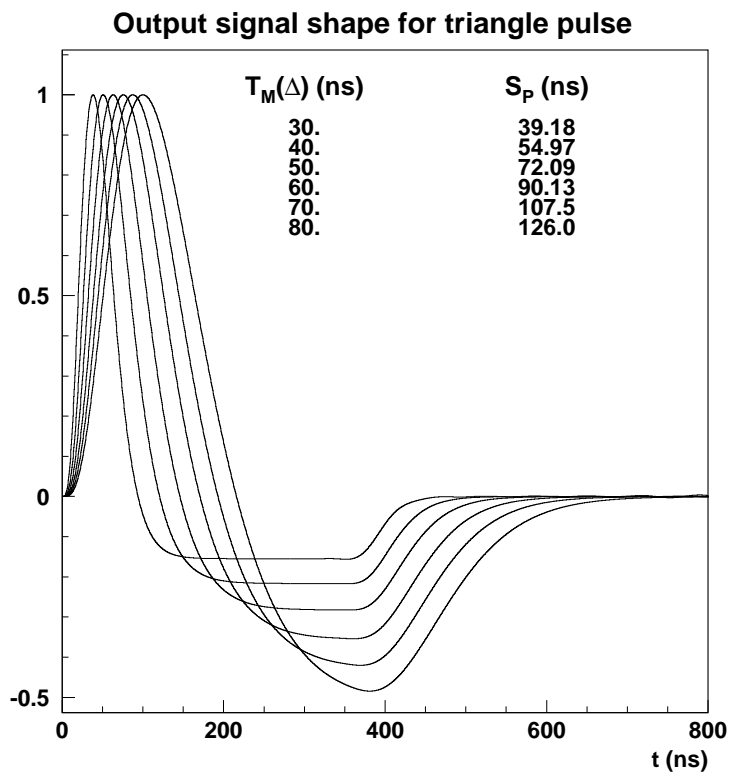


Figure 2: Example of output signal shapes  $g(t)$  for triangle pulses (see text).

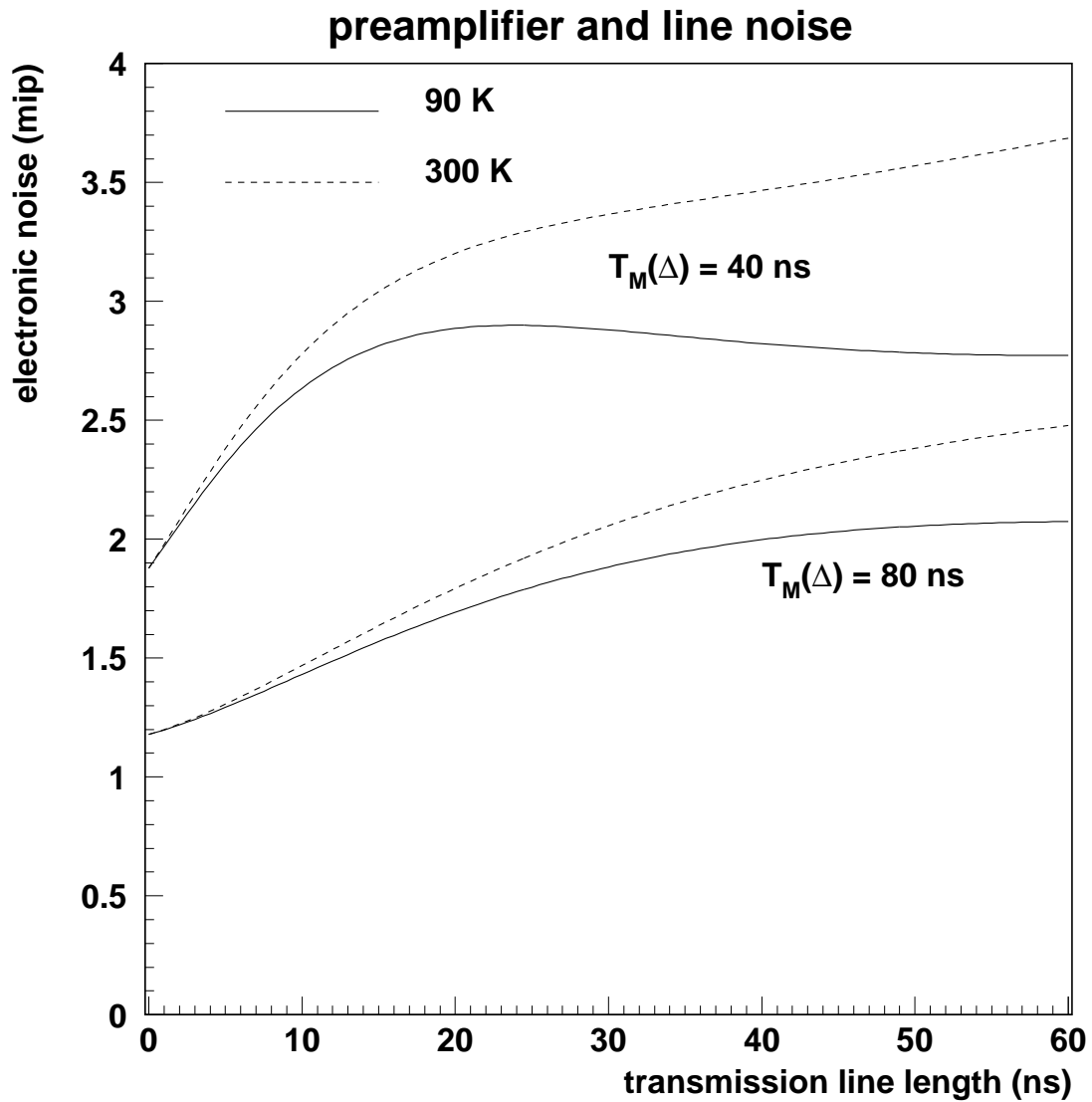


Figure 3: Electronic noise as a function of the transmission line length  $t_l$  for  $C_d = 124.9$  ns for two  $t_m(\Delta)$  and two line temperatures. The charge available from the EST cell (tile) considered here is 31024 electrons/mip.

$\eta$	preamplifiers				tiles				tiles/preamplifiers			
	1st	2nd	3rd	4th	1st	2nd	3rd	4th	1st	2nd	3rd	4th
1.525	8				8				1			
1.575	8	8			8	8			1	1		
1.625	8	16			8	16			1	1		
1.675	8	16	8		8	16	8		1	1	1	
1.725	8	16	16		8	16	16		1	1	1	
1.775	8	16	16	8	8	16	16	8	1	1	1	1
1.850	8	16	16	16	8	16	16	16	1	1	1	1
1.950	8	16	16	16	8	16	16	16	1	1	1	1
2.050	8	16	16	16	8	16	16	16	1	1	1	1
2.150	8	16	16	16	8	16	16	16	1	1	1	1
2.250	8	16	16	16	8	16	16	16	1	1	1	1
2.350	8	16	16	16	8	16	16	16	1	1	1	1
2.450	8	16	8	8	8	16	16	16	1	1	2	2
2.550	8	16	8	8	8	16	16	16	1	1	2	2
2.650	8	16	8	8	8	16	16	16	1	1	2	2
2.750	8	8	8	8	8	16	16	16	1	2	2	2
2.850	8	8	4	4	8	16	16	16	1	2	4	4
2.950	8	8	4	4	8	16	16	16	1	2	4	4
3.050	8	8	4	4	8	16	16	16	1	2	4	4
3.150	8	4			8	8			1	2		
total	160	252	180	148	160	288	248	216				

Table 1: Assumed number of preamplifiers and tiles in each readout channel.

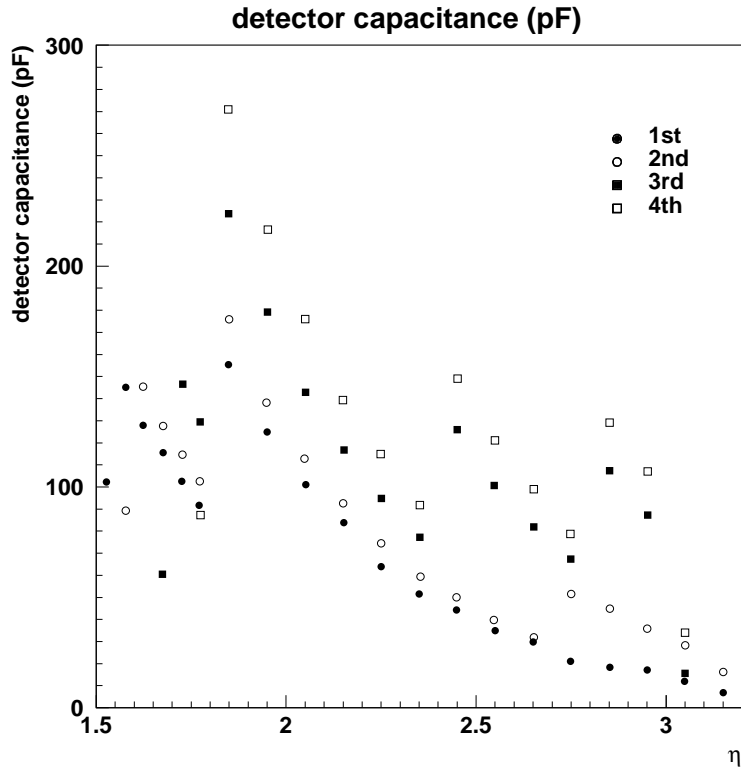


Figure 4: Detector capacitance associated with each preamplifier.

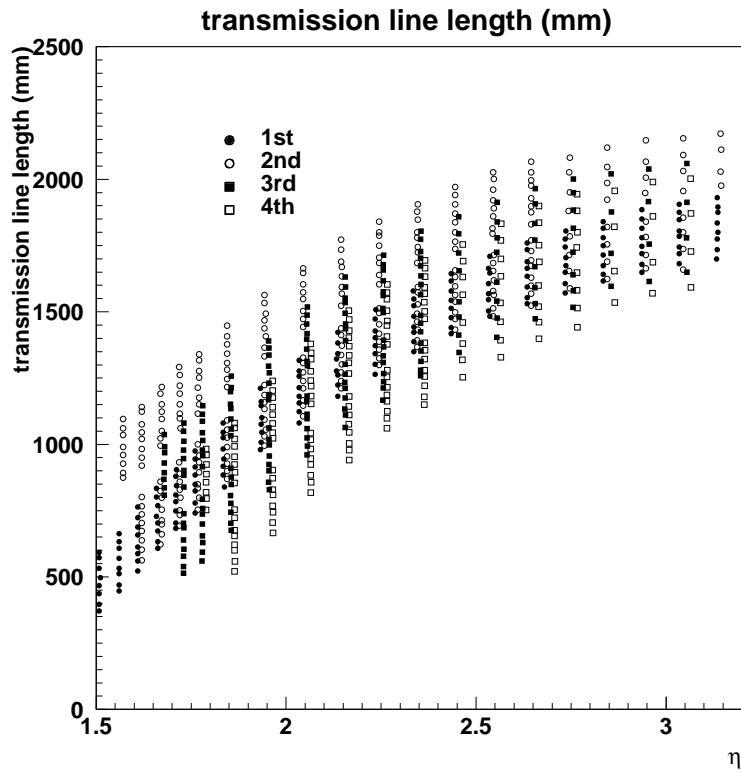


Figure 5: Transmission line length associated with each preamplifier.

### 3 Pileup Noise

Minimum bias events were generated with PYTHIA 5.7 [4]. Values of  $dN/d\eta = 6.5$  and  $\langle p_T \rangle = 558$  MeV for charged particles with  $p_T \geq 150$  MeV and  $|\eta| \leq 2.5$  were found. The resulting secondary particles were followed through the detector using the ATLAS software package DICE and the information about the energy deposition in each readout channel of the hadronic end-cap calorimeter was stored. The proposed depth segmentation 8:16:16:16 tiles was used. For a luminosity of  $1.0 \times 10^{34}$  cm<sup>-2</sup>s<sup>-1</sup>, a bunch spacing time of 25 ns and an inelastic cross section of p-p interactions at  $\sqrt{s}=14$  TeV of 70 mb the average number of events in one bunch crossing is 17.5. The multiplicity of the events in a bunch crossing was generated according to a Poisson distribution with this mean value. The energy depositions in the corresponding cells were summed up to form a cell energy for each bunch crossing.

The calibration parameter for the hadron calorimeter was determined by minimization of the energy resolution of jets in the end-cap region. The energy scale was set to the jet energy scale, found to be 26 times the energy deposited in the LAr in the end-cap hadronic calorimeter. From now on, energies quoted in GeV refer to GeV jet scale, unless otherwise specified.

Table 2 shows values obtained for  $\sigma_1$ , the rms of the energy deposited per bunch crossing, in different regions of  $\Delta\eta \times \Delta\phi = 0.1 \times \pi/32$ .  $\sigma_1$  is therefore the pileup noise from only one bunch crossing. Approximately 7300 bunch crossings were simulated for each entry. Note that  $\sigma_1$  obtained using all four depth compartments is bigger than the quadratic sum of the  $\sigma_1$  of each of the depth compartment because of longitudinal correlations in the energy deposition. These data were then parametrised as functions of  $\eta$  for each depth compartment, as shown in figures 6, 7, 8 and 9.

The segmentation proposed of the end-cap hadronic calorimeter is  $\Delta\eta \times \Delta\phi = 0.1 \times \pi/32$  for  $1.8 < \eta < 3.2$  and  $\Delta\eta \times \Delta\phi = 0.05 \times \pi/32$  for  $1.5 < \eta < 1.8$ . In order to estimate the pileup noise for regions with  $\Delta\eta = 0.05$ , we have assumed [5]

$$\sigma_1 \propto (\Delta\eta \Delta\phi)^{0.76}.$$

The pileup noise  $\sigma_p$  is then given by [5]

$$\sigma_p^2 = \sigma_1^2 \frac{S_p}{T_c} \quad (1)$$

where  $T_c = 25$  ns is the time between crossings. The pileup sum  $S_p$  is given by

$$S_p = T_c \sum_{i=-\infty}^{\infty} g^2(t_i)$$

where  $g(t)$  is the output signal shape, normalised to  $g(t_0) = g_{\max} = 1$ , and the sum runs over all bunch crossings. Examples of signal shapes  $g(t)$  are shown in figure 2 along with corresponding values of the pileup sum  $S_p$ .

Values of the pileup sum  $S_p$  were obtained for each readout channel as a function of  $t_p(\delta)$ , allowing the computation of the corresponding pileup noise using equation 1. (Another method consists of simulating many bunch crossings and using  $g(t_i)$  as crossing weights. Though this method reduces to equation 1 in the case of  $\sigma_p$ , it would be needed for the study of non-gaussian effects.)

readout depth	$\sigma_1$ (GeV) in $\Delta\eta = 0.1$ regions			
	$\eta = 1.75$	$\eta = 2.25$	$\eta = 2.55$	$\eta = 3.05$
1st	0.202	0.339	0.376	1.41
2nd	0.114	0.258	0.296	0.650
3rd	0.0569	0.0849	0.0919	0.217
4th	0.00538	0.0372	0.0526	0.110
all	0.261	0.493	0.551	1.72

Table 2: Values of  $\sigma_1$ , the rms of the energy deposited per bunch crossing, in four  $\Delta\eta \times \Delta\phi = 0.1 \times \pi/32$  regions for each and all depth compartments.

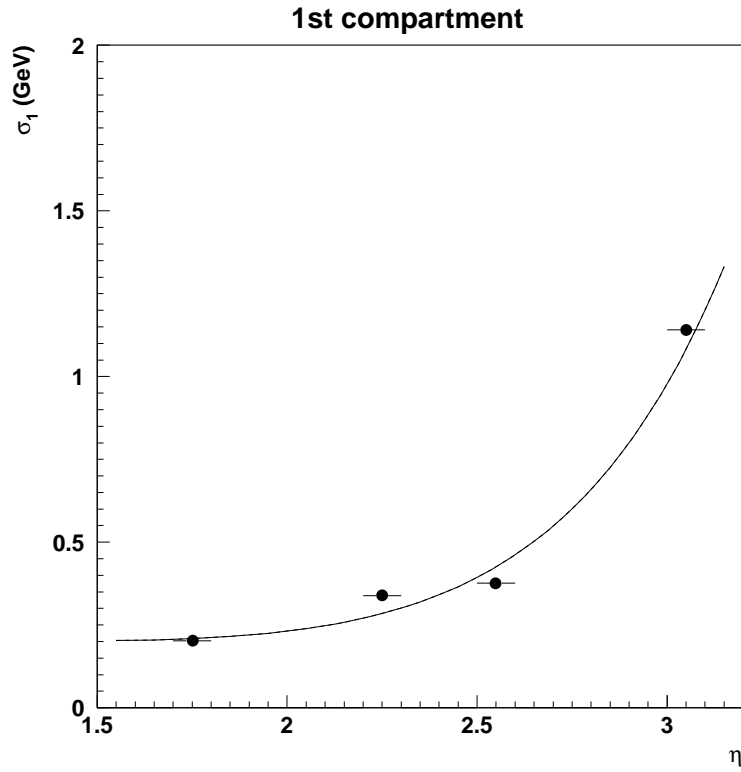


Figure 6: Pileup noise from one bunch crossing for the first readout depth.

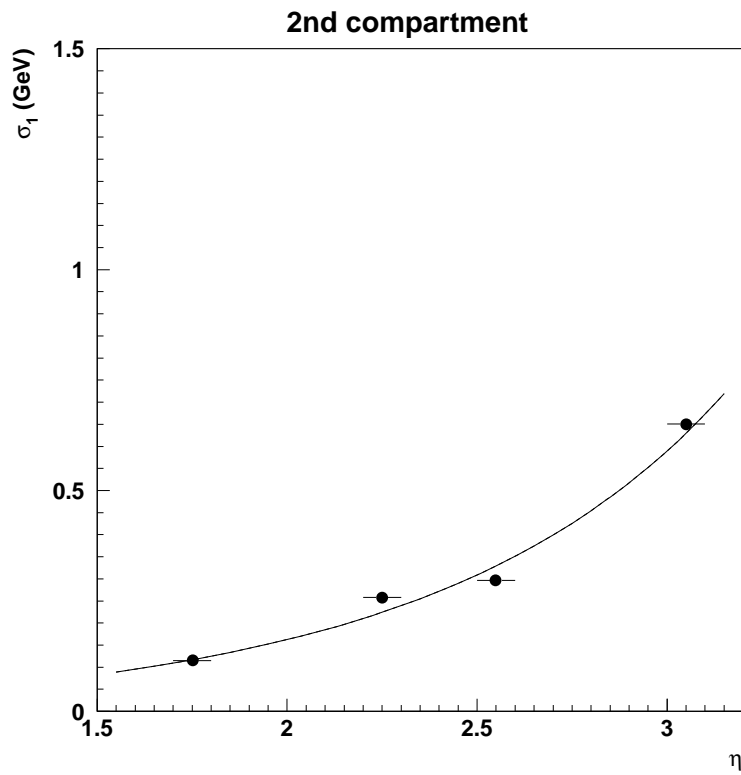


Figure 7: Pileup noise from one bunch crossing for the second readout depth.

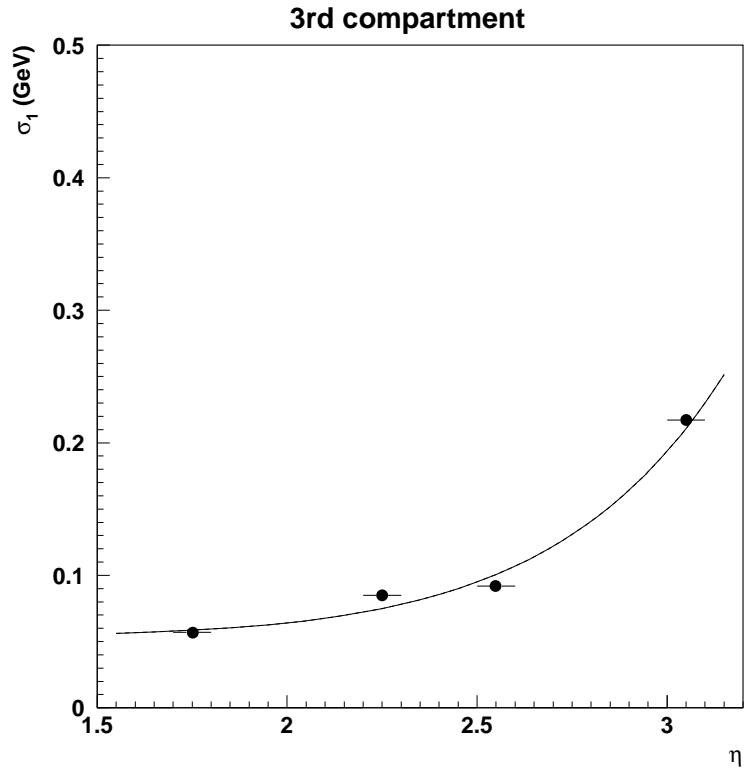


Figure 8: Pileup noise from one bunch crossing for the third readout depth.

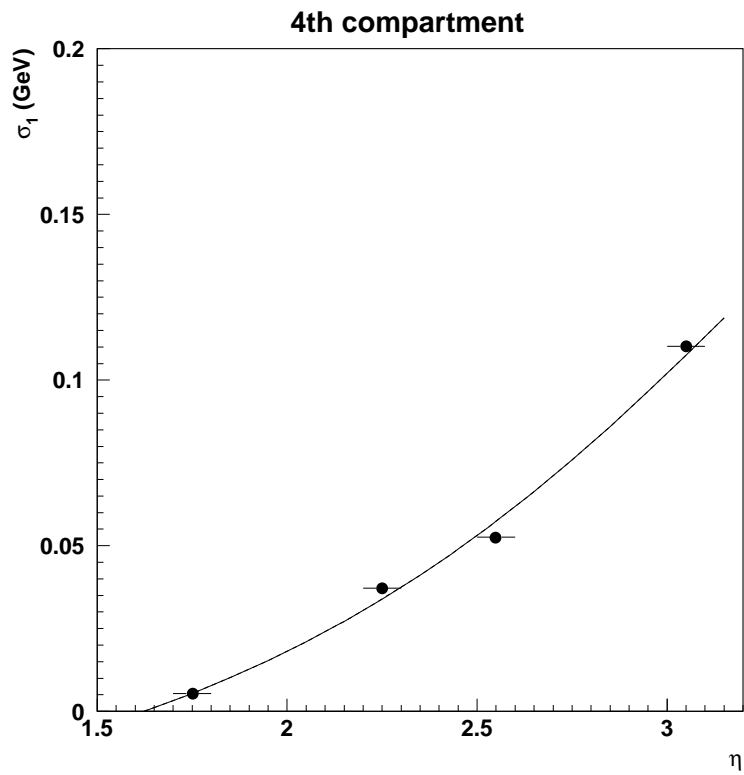


Figure 9: Pileup noise from one bunch crossing for the fourth readout depth.

## 4 Total Noise and Optimum $t_p(\delta)$

### 4.1 Optimum $t_p(\delta)$

Using the electronic noise and the pileup noise for each compartment as a function of  $t_p(\delta)$ , we can estimate the optimum  $t_p(\delta)$  needed in order to minimise the total noise for minimum ionising particles. To this end, the electronic noise is converted from rms electrons to GeV (jet scale) using the factors 26 (GeV jet scale)/(GeV deposited) and 23.6 (eV deposited)/(rms electrons).

Figures 10, 11, 12 and 13 shows the behaviour of the electronic, pileup and total noise as a function of  $t_p(\delta)$  for the four readout compartments at  $\eta = 2.25$ . The pileup noise is more important in the front compartment and increases with  $t_p(\delta)$  while the electronic noise decreases with  $t_p(\delta)$ . The electronic noise is also a function of the detector capacitance, of the ganging scenario and of the transmission line length. In order to estimate the noise in units of mips (average energy deposited by a minimum ionising particle in the calorimeter), the thickness of active LAr for each readout channel, shown in table 3, was used. Also, 2.11 MeV/cm for a mip in LAr was assumed.

The  $t_p(\delta)$  optimisation was performed for  $20 \text{ ns} < t_p(\delta) < 50 \text{ ns}$ . Therefore a value of  $t_p(\delta)$  of 20 ns indicates that the optimum  $t_p(\delta)$  is less than or equal to 20 ns. This is the case when the pileup noise dominates. A value of  $t_p(\delta)$  of 50 ns indicates that the optimum  $t_p(\delta)$  is more than or equal to 50 ns. This is the case when the electronic noise dominates. Figure 14 shows the optimum  $t_p(\delta)$  obtained. The noise in the first compartments is dominated by pileup while the fourth compartments have significant electronic noise. The corresponding signal peaking times are shown in figure 15. Effects of the detector capacitance (in general bigger for low  $\eta$ ), of the assumed ganging scenario and of the various optimum  $t_p(\delta)$  can be seen.

The electronic noise at optimum  $t_p(\delta)$  is plotted in figure 16 in GeV and in figure 17 in mip. The corresponding results for the pileup noise are shown in figures 18 and 19. The total noise is shown in figure 20 and as signal over noise for a mip in figure 21. Details of the numerical values of the results can be found in tables 4 and 5.

### 4.2 Choosing values of $t_p(\delta)$

Clearly we do not wish to have too many different  $t_p(\delta)$  for the channels of the hadronic end-cap calorimeter. We must therefore choose some values, guided by the optimum  $t_p(\delta)$ . Assuming that it is possible to have different  $t_p(\delta)$  for different depth compartments of the same  $\eta, \phi$  region (which is not obvious especially with regards to building a trigger signal), a set of four  $t_p(\delta)$  were chosen following the rule

- 20 ns if  $t_p(\delta)(\text{optimum}) \leq 25 \text{ ns}$ ;
- 30 ns if  $25 \text{ ns} < t_p(\delta)(\text{optimum}) \leq 35 \text{ ns}$ ;
- 40 ns if  $35 \text{ ns} < t_p(\delta)(\text{optimum}) \leq 45 \text{ ns}$ ;
- 50 ns if  $45 \text{ ns} < t_p(\delta)(\text{optimum})$ .

In general, an excess noise results from this compromise. The excess electronic, pileup and total noise for these chosen  $t_p(\delta)$  are shown in figures 22, 23 and 24 respectively.

$\eta$	readout depth			
	1st	2nd	3rd	4th
1.525	61.0			
1.575	60.5	60.5		
1.625	60.0	120.0		
1.675	59.6	119.1	59.6	
1.725	59.2	118.3	118.3	
1.775	58.8	117.6	117.6	58.8
1.850	58.3	116.7	116.7	116.7
1.950	57.8	115.6	115.6	115.6
2.050	57.4	114.8	114.8	114.8
2.150	57.0	114.1	114.1	114.1
2.250	56.8	113.5	113.5	113.5
2.350	56.5	113.1	113.1	113.1
2.450	56.4	112.7	112.7	112.7
2.550	56.2	112.4	112.4	112.4
2.650	56.1	112.2	112.2	112.2
2.750	56.0	112.0	112.0	112.0
2.850	55.9	111.8	111.8	111.8
2.950	55.8	111.7	111.7	111.7
3.050	55.8	111.5	111.5	111.5
3.150	55.7	55.7		

Table 3: Thickness (mm) of active LAr for each readout channel as seen from the centre of the ATLAS detector.

While the electronic noise and the pileup noise can vary by as much as 20% and 10% respectively, the total noise is found to increase very little (less than 3%). Details of the numerical values corresponding to the chosen  $t_p(\delta)$  can be found in tables 6 and 7.

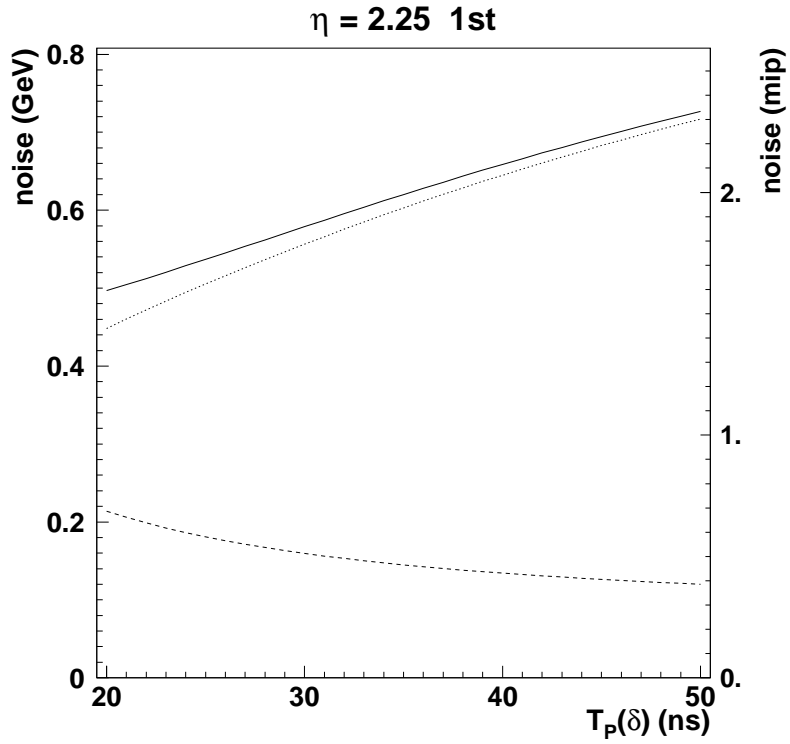


Figure 10: Total, electronic (dashes) and pileup (dots) noise as a function of  $t_p(\delta)$  in the first compartment at  $\eta = 2.25$ .

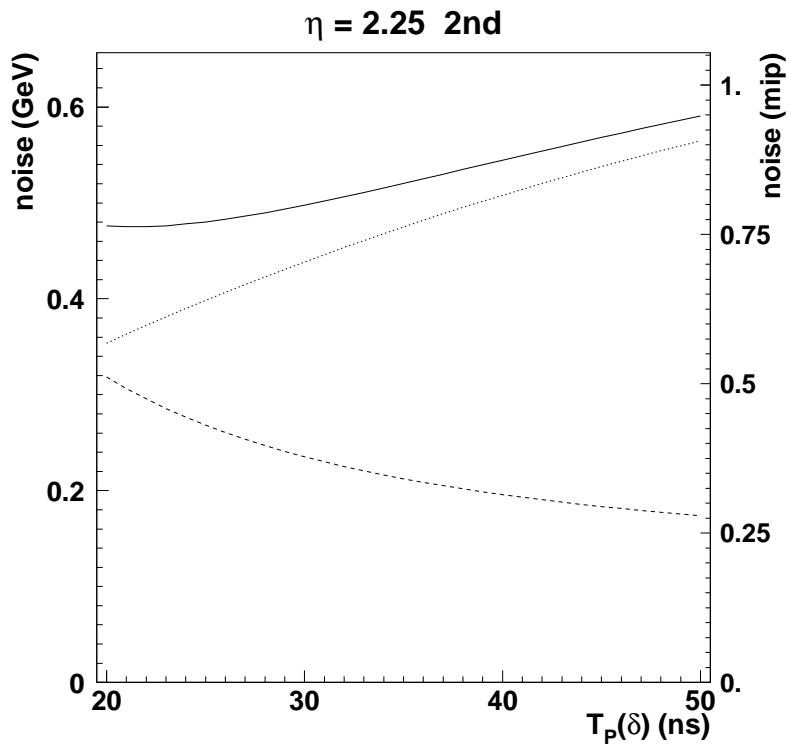


Figure 11: Total, electronic (dashes) and pileup (dots) noise as a function of  $t_p(\delta)$  in the second compartment at  $\eta = 2.25$ .

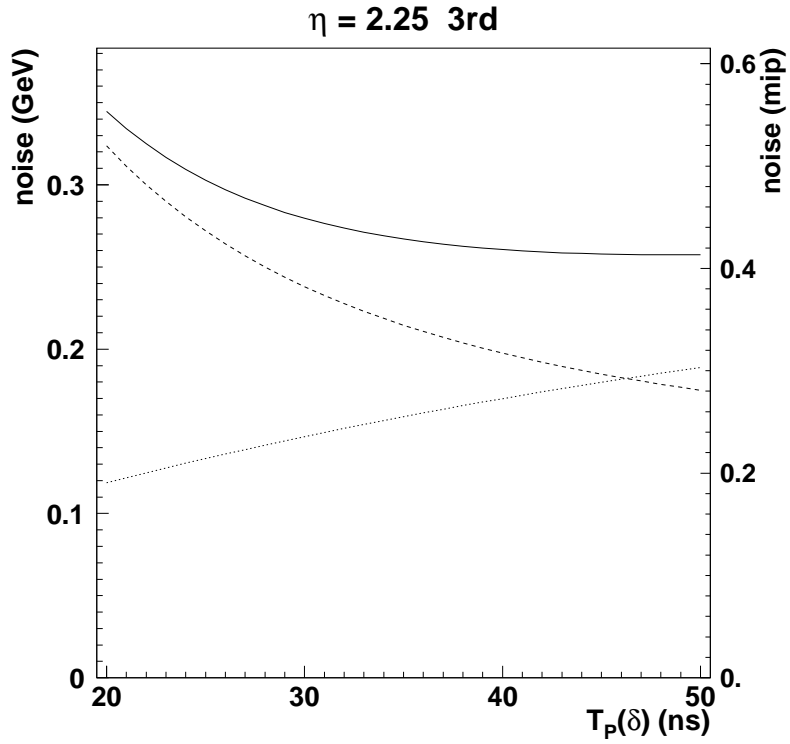


Figure 12: Total, electronic (dashes) and pileup (dots) noise as a function of  $t_p(\delta)$  in the third compartment at  $\eta = 2.25$ .

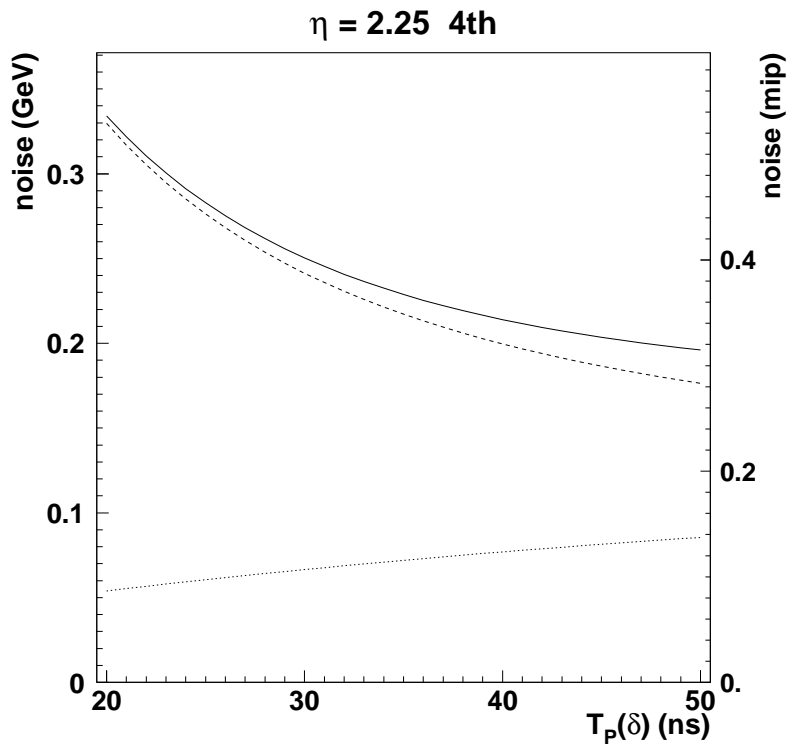


Figure 13: Total, electronic (dashes) and pileup (dots) noise as a function of  $t_p(\delta)$  in the fourth compartment at  $\eta = 2.25$ .

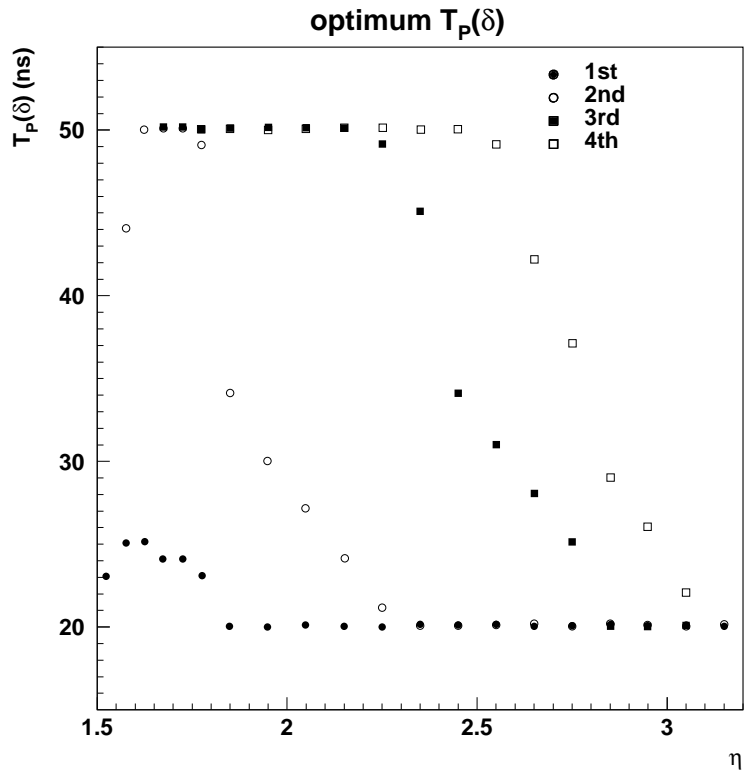


Figure 14: Optimum  $t_p(\delta)$  values. The search for optimum  $t_p(\delta)$  was done between 20 ns and 50 ns.

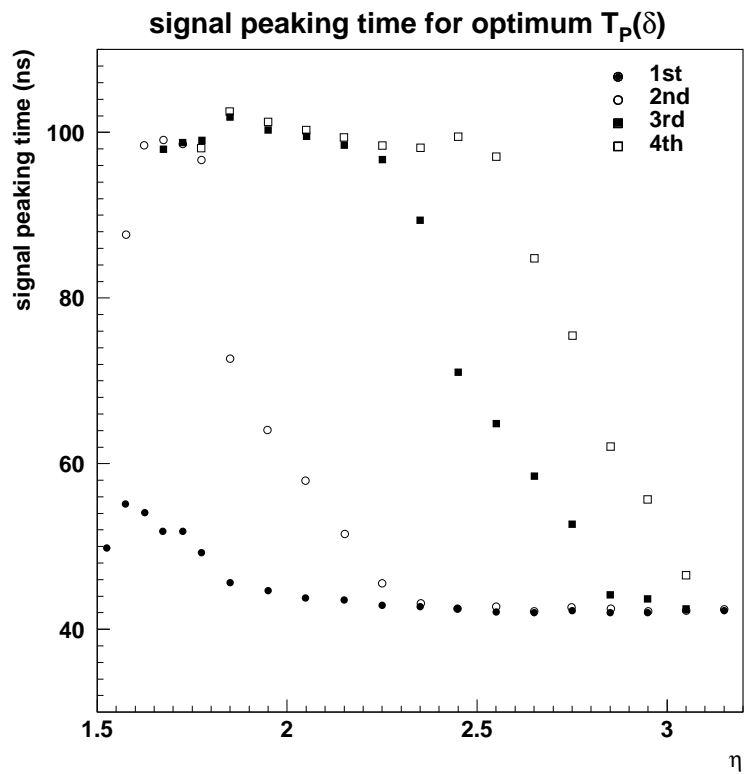


Figure 15: Signal peaking times at optimum  $t_p(\delta)$ .

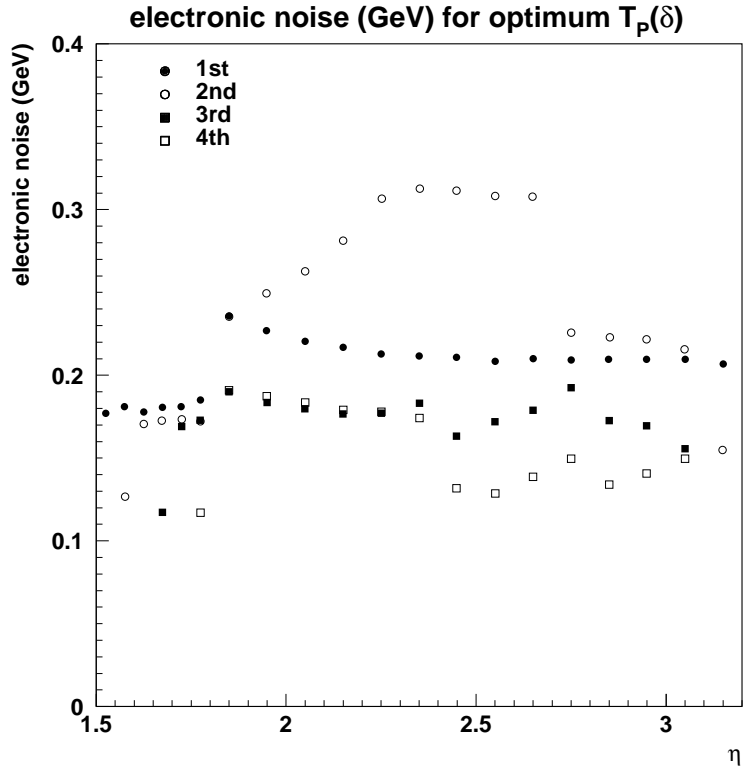


Figure 16: Electronic noise (GeV) at optimum  $t_p(\delta)$ .

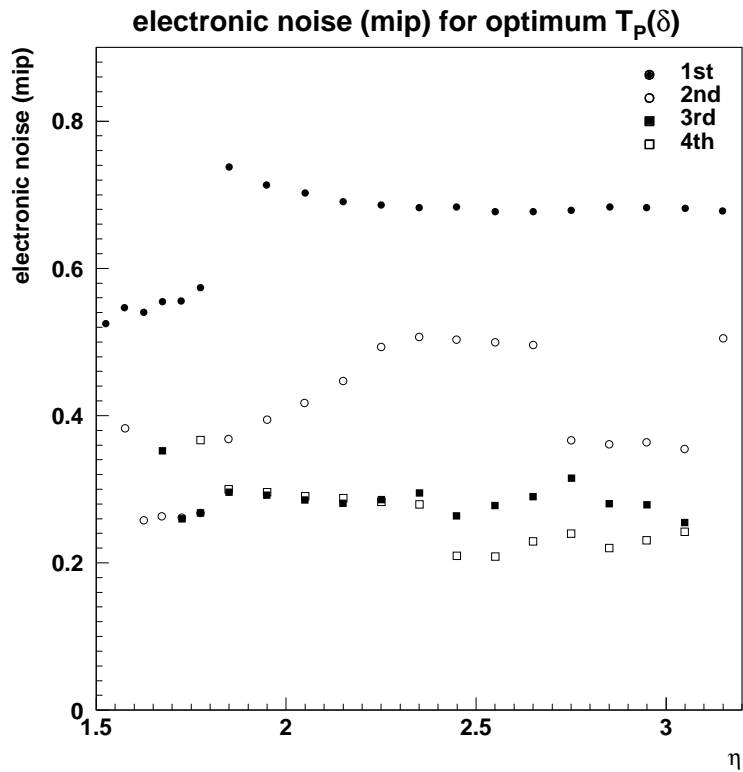


Figure 17: Electronic noise (mip) at optimum  $t_p(\delta)$ .

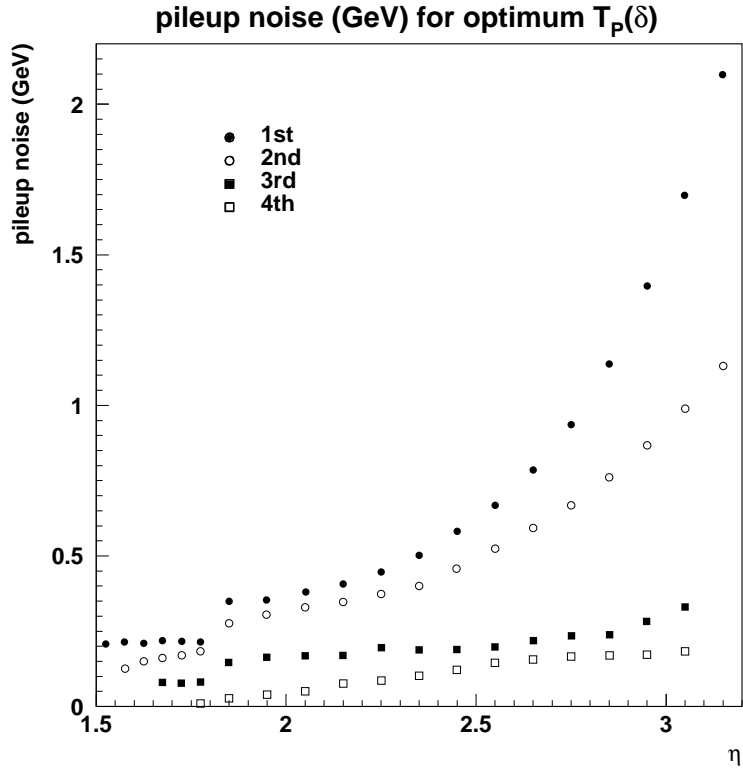


Figure 18: Pileup noise (GeV) at optimum  $t_p(\delta)$ .

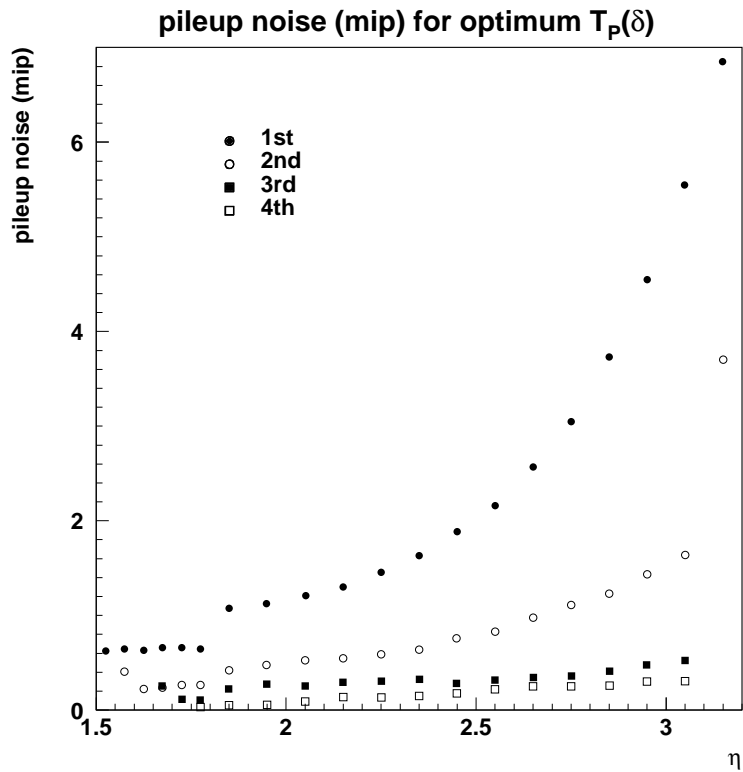


Figure 19: Pileup noise (mip) at optimum  $t_p(\delta)$ .

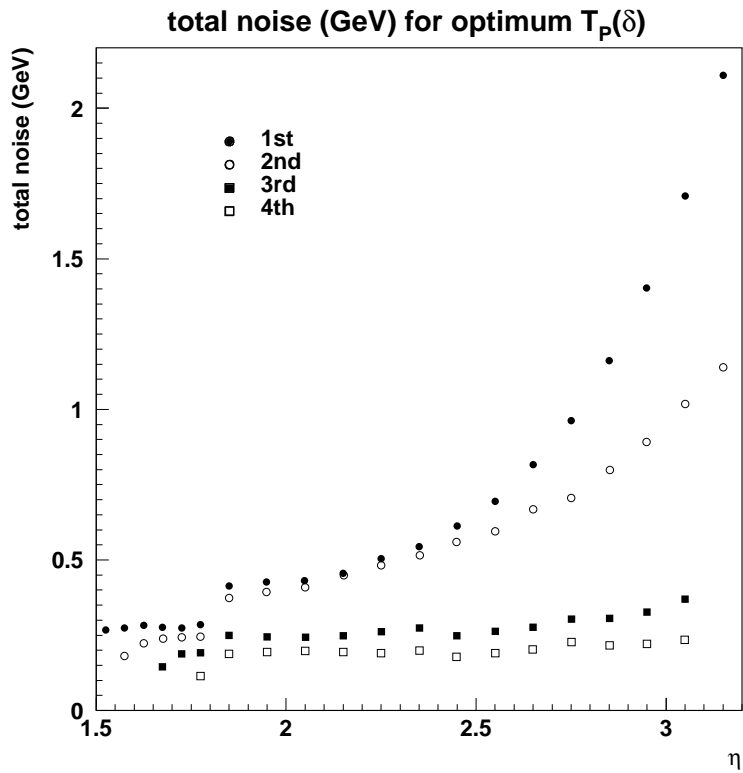


Figure 20: Total noise (GeV) at optimum  $t_p(\delta)$ .

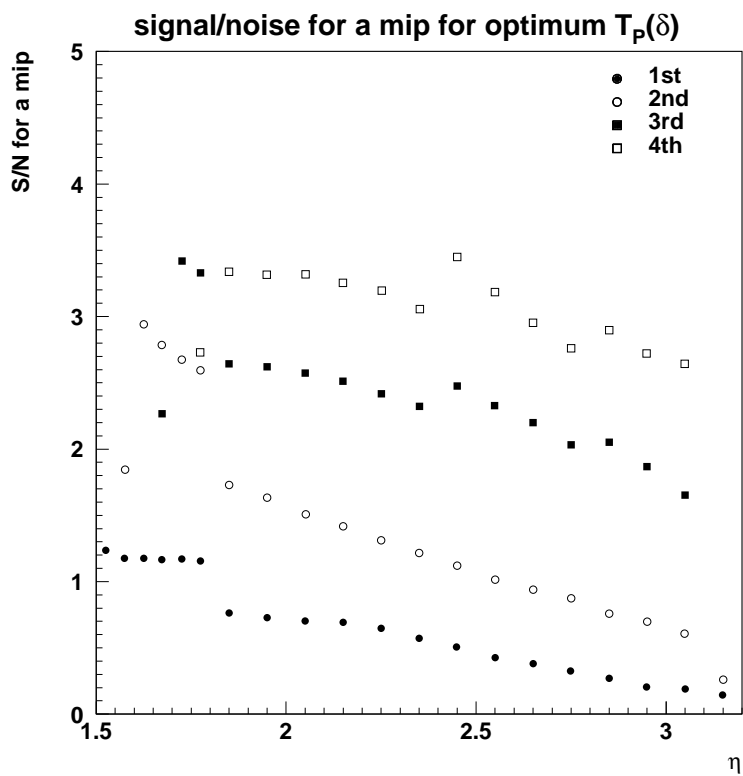


Figure 21: Signal over total noise at optimum  $t_p(\delta)$  for a mip.

$\eta$	comp	$t_p(\delta)$ (ns)	$t_m(\delta)$ (ns)	$t_m(\Delta)$ (ns)	elec (GeV)	pileup (GeV)	total (GeV)	elec (mip)	pileup (mip)	total (mip)
3.15	1	20	20.1	42.0	.2074	2.0918	2.1020	.6783	6.8425	6.8761
3.15	2	20	20.2	42.1	.1553	1.1286	1.1392	.5079	3.6918	3.7266
3.05	1	20	20.2	42.1	.2086	1.7000	1.7127	.6818	5.5564	5.5981
3.05	2	20	20.3	42.1	.2159	.9888	1.0121	.3528	1.6160	1.6540
3.05	3	20	20.8	42.4	.1555	.3314	.3661	.2541	.5416	.5983
3.05	4	22	23.4	46.7	.1482	.1783	.2318	.2421	.2914	.3788
2.95	1	20	20.2	42.1	.2085	1.3872	1.4028	.6807	4.5297	4.5805
2.95	2	20	20.7	42.3	.2209	.8675	.8952	.3606	1.4163	1.4615
2.95	3	20	22.6	43.7	.1691	.2818	.3286	.2761	.4600	.5365
2.95	4	26	29.1	55.7	.1406	.1757	.2250	.2296	.2869	.3674
2.85	1	20	20.3	42.1	.2084	1.1391	1.1580	.6798	3.7148	3.7765
2.85	2	20	21.0	42.5	.2230	.7620	.7939	.3636	1.2425	1.2946
2.85	3	20	23.4	44.4	.1738	.2412	.2973	.2835	.3933	.4848
2.85	4	29	32.9	62.1	.1332	.1661	.2129	.2172	.2709	.3472
2.75	1	20	20.3	42.1	.2086	.9430	.9658	.6792	3.0709	3.1452
2.75	2	20	21.3	42.7	.2257	.6700	.7070	.3675	1.0910	1.1512
2.75	3	25	26.6	52.7	.1924	.2323	.3016	.3133	.3782	.4911
2.75	4	37	38.8	75.3	.1481	.1655	.2221	.2411	.2694	.3616
2.65	1	20	20.5	42.2	.2089	.7888	.8160	.6790	2.5641	2.6525
2.65	2	20	20.6	42.3	.3063	.5880	.6630	.4978	.9557	1.0776
2.65	3	28	30.1	58.8	.1800	.2151	.2804	.2925	.3496	.4558
2.65	4	42	44.3	84.6	.1391	.1541	.2076	.2260	.2505	.3374
2.55	1	20	20.6	42.3	.2095	.6683	.7003	.6794	2.1674	2.2714
2.55	2	20	20.9	42.4	.3081	.5174	.6022	.4997	.8391	.9767
2.55	3	31	33.7	64.9	.1705	.2005	.2632	.2765	.3252	.4269
2.55	4	49	51.8	97.2	.1294	.1434	.1932	.2099	.2326	.3133
2.45	1	20	20.9	42.4	.2104	.5747	.6120	.6805	1.8590	1.9797
2.45	2	20	21.2	42.6	.3106	.4556	.5514	.5024	.7368	.8918
2.45	3	34	37.5	71.0	.1634	.1884	.2494	.2643	.3048	.4034
2.45	4	50	53.8	99.6	.1305	.1237	.1798	.2110	.2001	.2908
2.35	1	20	21.2	42.6	.2118	.5029	.5457	.6828	1.6213	1.7592
2.35	2	20	21.6	42.9	.3140	.4013	.5095	.5061	.6469	.8214
2.35	3	45	46.4	89.4	.1831	.1956	.2679	.2951	.3153	.4319
2.35	4	50	51.8	98.2	.1745	.1037	.2030	.2813	.1672	.3272

Table 4: Optimum values of  $t_p(\delta)$  and corresponding signal peaking times  $t_m(\delta)$  and  $t_m(\Delta)$ , and noise contributions in GeV jet scale and in mip.

$\eta$	comp	$t_p(\delta)$ (ns)	$t_m(\delta)$ (ns)	$t_m(\Delta)$ (ns)	elec (GeV)	pileup (GeV)	total (GeV)	elec (mip)	pileup (mip)	total (mip)
2.25	1	20	21.7	42.9	.2139	.4484	.4968	.6868	1.4398	1.5952
2.25	2	21	23.1	45.2	.3065	.3632	.4753	.4921	.5832	.7630
2.25	3	49	50.9	96.6	.1768	.1871	.2574	.2838	.3003	.4132
2.25	4	50	52.5	98.7	.1764	.0855	.1960	.2832	.1372	.3147
2.15	1	20	22.2	43.4	.2169	.4078	.4619	.6929	1.3030	1.4758
2.15	2	24	26.6	51.5	.2813	.3436	.4440	.4494	.5489	.7094
2.15	3	50	52.6	98.7	.1770	.1759	.2495	.2827	.2810	.3986
2.15	4	50	53.5	99.3	.1790	.0687	.1917	.2859	.1097	.3062
2.05	1	20	22.9	43.9	.2211	.3785	.4383	.7022	1.2020	1.3921
2.05	2	27	30.4	57.8	.2628	.3219	.4155	.4174	.5112	.6599
2.05	3	50	53.6	99.4	.1797	.1660	.2446	.2853	.2636	.3884
2.05	4	50	54.7	100.2	.1825	.0532	.1901	.2898	.0844	.3018
1.95	1	20	23.7	44.7	.2269	.3581	.4239	.7153	1.1291	1.3366
1.95	2	30	34.3	64.2	.2495	.2996	.3898	.3933	.4722	.6145
1.95	3	50	54.9	100.3	.1834	.1585	.2424	.2891	.2499	.3821
1.95	4	50	56.3	101.4	.1873	.0389	.1913	.2952	.0614	.3016
1.85	1	20	24.7	45.8	.2348	.3452	.4175	.7338	1.0787	1.3046
1.85	2	34	39.4	72.6	.2350	.2812	.3665	.3672	.4394	.5726
1.85	3	50	56.6	101.6	.1885	.1530	.2428	.2945	.2391	.3793
1.85	4	50	57.5	102.4	.1903	.0258	.1920	.2973	.0403	.3000
1.78	1	23	25.4	49.4	.1844	.2110	.2802	.5715	.6539	.8685
1.78	2	49	51.2	96.7	.1730	.1780	.2482	.2681	.2758	.3847
1.78	3	50	53.1	99.0	.1725	.0877	.1935	.2674	.1359	.2999
1.78	4	50	51.5	98.0	.1178	.0097	.1182	.3651	.0302	.3663
1.73	1	24	26.8	51.6	.1802	.2134	.2793	.5553	.6575	.8606
1.73	2	50	52.6	98.7	.1722	.1681	.2407	.2653	.2590	.3708
1.73	3	50	52.2	98.5	.1689	.0865	.1897	.2602	.1332	.2923
1.68	1	24	27.2	52.0	.1819	.2117	.2791	.5566	.6480	.8542
1.68	2	50	53.1	99.0	.1733	.1573	.2341	.2652	.2407	.3582
1.68	3	50	50.8	97.6	.1161	.0854	.1441	.3552	.2612	.4409
1.63	1	25	28.7	54.3	.1785	.2151	.2796	.5424	.6536	.8493
1.63	2	50	52.4	98.6	.1702	.1469	.2249	.2586	.2232	.3416
1.58	1	25	29.2	54.8	.1808	.2146	.2806	.5449	.6467	.8457
1.58	2	44	45.7	87.7	.1261	.1292	.1805	.3799	.3894	.5440
1.53	1	23	25.8	49.7	.1762	.2036	.2692	.5261	.6079	.8040

Table 5: Optimum values (continued) of  $t_p(\delta)$  and corresponding signal peaking times  $t_m(\delta)$  and  $t_m(\Delta)$ , and noise contributions in GeV jet scale and in mip.

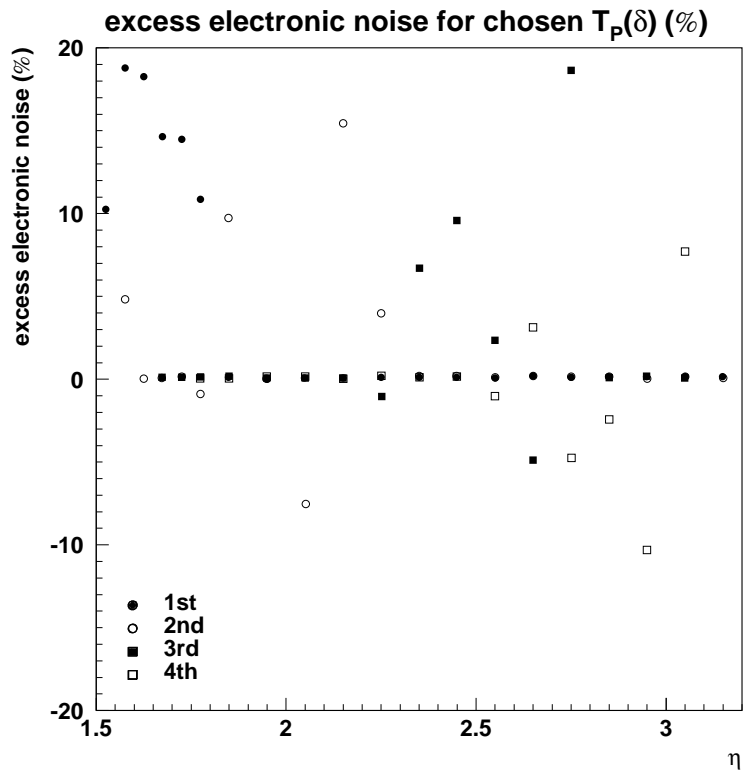


Figure 22: Excess electronic noise for chosen  $t_p(\delta)$ .

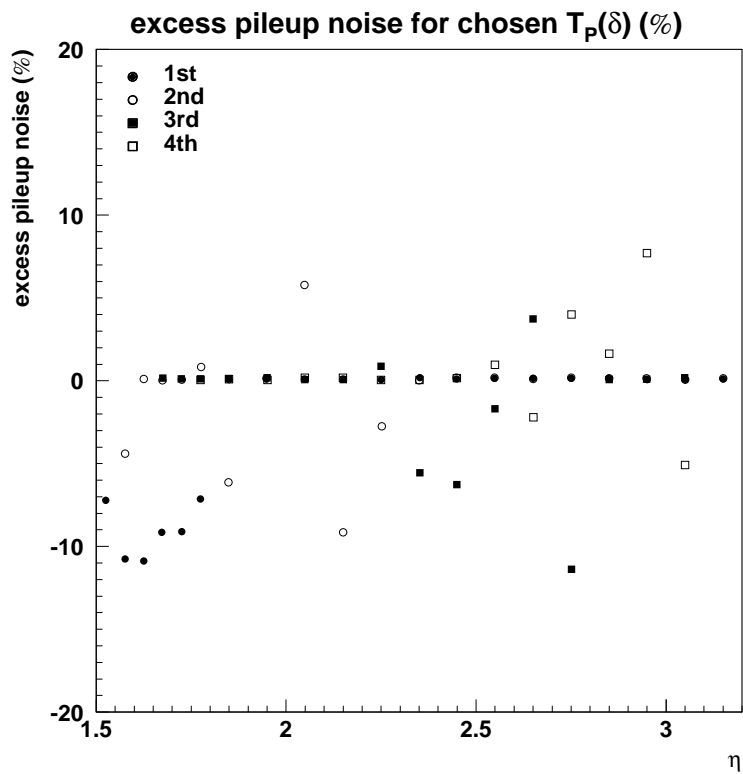


Figure 23: Excess pileup noise for chosen  $t_p(\delta)$ .

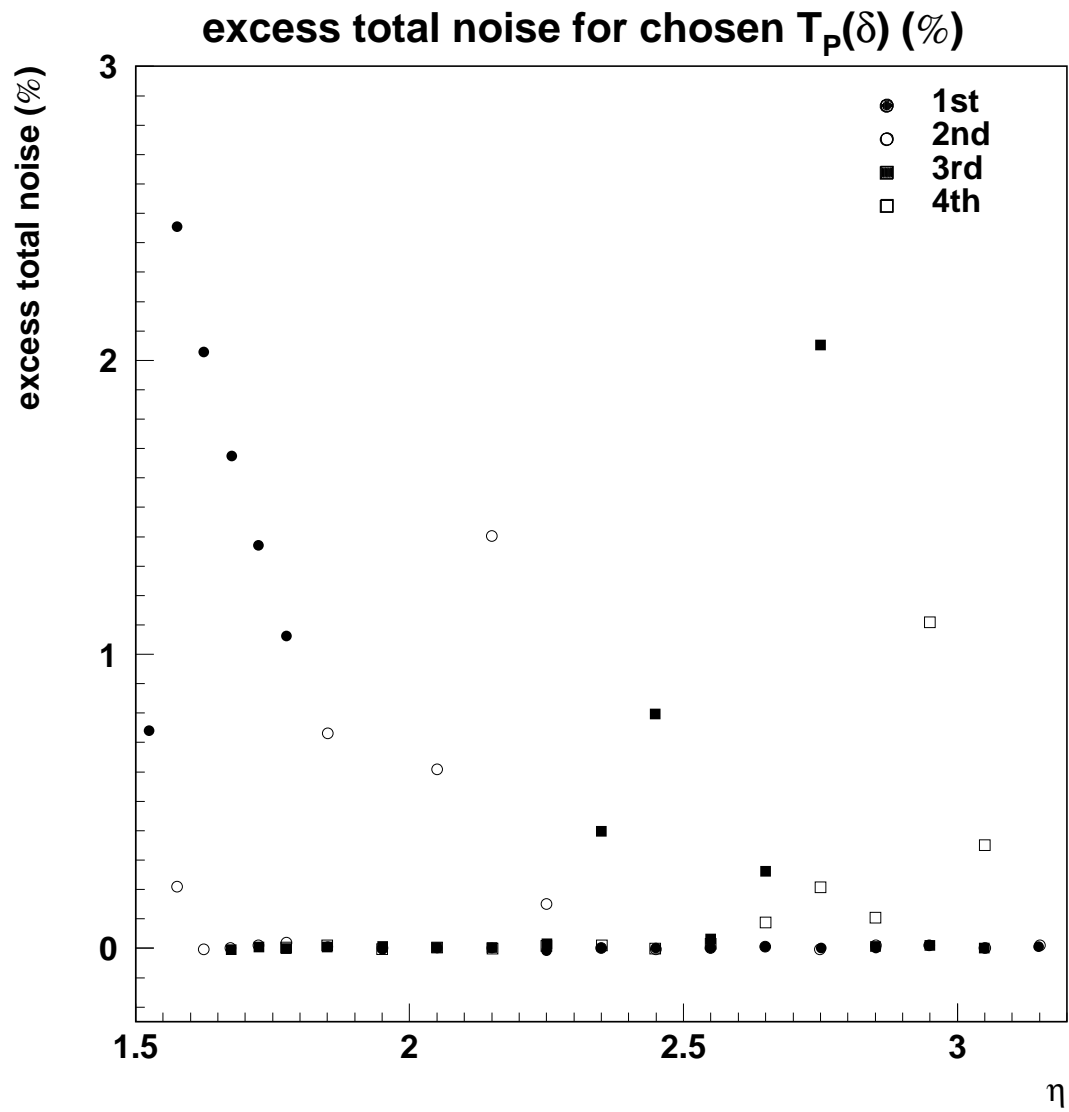


Figure 24: Excess total noise for chosen  $t_p(\delta)$ .

$\eta$	comp	$t_p(\delta)$ (ns)	$t_m(\delta)$ (ns)	$t_m(\Delta)$ (ns)	elec (GeV)	pileup (GeV)	total (GeV)	elec (mip)	pileup (mip)	total (mip)
3.15	1	20	20.1	42.0	.2074	2.0918	2.1020	.6783	6.8425	6.8761
3.15	2	20	20.2	42.1	.1553	1.1286	1.1392	.5079	3.6918	3.7266
3.05	1	20	20.2	42.1	.2086	1.7000	1.7127	.6818	5.5564	5.5981
3.05	2	20	20.3	42.1	.2159	.9888	1.0121	.3528	1.6160	1.6540
3.05	3	20	20.8	42.4	.1555	.3314	.3661	.2541	.5416	.5983
3.05	4	20	21.4	42.8	.1596	.1693	.2326	.2608	.2766	.3802
2.95	1	20	20.2	42.1	.2085	1.3872	1.4028	.6807	4.5297	4.5805
2.95	2	20	20.7	42.3	.2209	.8675	.8952	.3606	1.4163	1.4615
2.95	3	20	22.6	43.7	.1691	.2818	.3286	.2761	.4600	.5365
2.95	4	30	33.0	63.2	.1262	.1893	.2275	.2061	.3091	.3715
2.85	1	20	20.3	42.1	.2084	1.1391	1.1580	.6798	3.7148	3.7765
2.85	2	20	21.0	42.5	.2230	.7620	.7939	.3636	1.2425	1.2946
2.85	3	20	23.4	44.4	.1738	.2412	.2973	.2835	.3933	.4848
2.85	4	30	33.9	63.9	.1298	.1691	.2132	.2117	.2757	.3476
2.75	1	20	20.3	42.1	.2086	.9430	.9658	.6792	3.0709	3.1452
2.75	2	20	21.3	42.7	.2257	.6700	.7070	.3675	1.0910	1.1512
2.75	3	20	21.8	43.1	.2286	.2062	.3078	.3722	.3357	.5012
2.75	4	40	41.7	80.7	.1411	.1720	.2225	.2298	.2801	.3623
2.65	1	20	20.5	42.2	.2089	.7888	.8160	.6790	2.5641	2.6525
2.65	2	20	20.6	42.3	.3063	.5880	.6630	.4978	.9557	1.0776
2.65	3	30	32.0	62.5	.1712	.2230	.2812	.2783	.3625	.4570
2.65	4	40	42.3	81.1	.1432	.1505	.2078	.2328	.2446	.3377
2.55	1	20	20.6	42.3	.2095	.6683	.7003	.6794	2.1674	2.2714
2.55	2	20	20.9	42.4	.3081	.5174	.6022	.4997	.8391	.9767
2.55	3	30	32.7	63.0	.1746	.1971	.2633	.2831	.3197	.4270
2.55	4	50	52.8	98.9	.1280	.1447	.1932	.2076	.2347	.3134
2.45	1	20	20.9	42.4	.2104	.5747	.6120	.6805	1.8590	1.9797
2.45	2	20	21.2	42.6	.3106	.4556	.5514	.5024	.7368	.8918
2.45	3	30	33.6	63.7	.1789	.1767	.2514	.2893	.2858	.4066
2.45	4	50	53.8	99.6	.1305	.1237	.1798	.2110	.2001	.2908
2.35	1	20	21.2	42.6	.2118	.5029	.5457	.6828	1.6213	1.7592
2.35	2	20	21.6	42.9	.3140	.4013	.5095	.5061	.6469	.8214
2.35	3	40	41.5	80.6	.1954	.1848	.2689	.3150	.2978	.4335
2.35	4	50	51.8	98.2	.1745	.1037	.2030	.2813	.1672	.3272

Table 6: Chosen values of  $t_p(\delta)$  and corresponding signal peaking times  $t_m(\delta)$  and  $t_m(\Delta)$ , and noise contributions in GeV jet scale and in mip.

$\eta$	comp	$t_p(\delta)$ (ns)	$t_m(\delta)$ (ns)	$t_m(\Delta)$ (ns)	elec (GeV)	pileup (GeV)	total (GeV)	elec (mip)	pileup (mip)	total (mip)
2.25	1	20	21.7	42.9	.2139	.4484	.4968	.6868	1.4398	1.5952
2.25	2	20	22.1	43.3	.3185	.3537	.4760	.5113	.5679	.7642
2.25	3	50	51.9	98.3	.1750	.1888	.2574	.2809	.3031	.4133
2.25	4	50	52.5	98.7	.1764	.0855	.1960	.2832	.1372	.3147
2.15	1	20	22.2	43.4	.2169	.4078	.4619	.6929	1.3030	1.4758
2.15	2	20	22.8	43.8	.3246	.3120	.4503	.5186	.4985	.7194
2.15	3	50	52.6	98.7	.1770	.1759	.2495	.2827	.2810	.3986
2.15	4	50	53.5	99.3	.1790	.0687	.1917	.2859	.1097	.3062
2.05	1	20	22.9	43.9	.2211	.3785	.4383	.7022	1.2020	1.3921
2.05	2	30	33.2	63.4	.2432	.3400	.4181	.3863	.5400	.6639
2.05	3	50	53.6	99.4	.1797	.1660	.2446	.2853	.2636	.3884
2.05	4	50	54.7	100.2	.1825	.0532	.1901	.2898	.0844	.3018
1.95	1	20	23.7	44.7	.2269	.3581	.4239	.7153	1.1291	1.3366
1.95	2	30	34.3	64.2	.2495	.2996	.3898	.3933	.4722	.6145
1.95	3	50	54.9	100.3	.1834	.1585	.2424	.2891	.2499	.3821
1.95	4	50	56.3	101.4	.1873	.0389	.1913	.2952	.0614	.3016
1.85	1	20	24.7	45.8	.2348	.3452	.4175	.7338	1.0787	1.3046
1.85	2	30	35.5	65.5	.2579	.2642	.3692	.4029	.4127	.5768
1.85	3	50	56.6	101.6	.1885	.1530	.2428	.2945	.2391	.3793
1.85	4	50	57.5	102.4	.1903	.0258	.1920	.2973	.0403	.3000
1.78	1	20	22.6	43.6	.2045	.1958	.2831	.6339	.6070	.8777
1.78	2	50	52.1	98.4	.1713	.1796	.2482	.2656	.2784	.3847
1.78	3	50	53.1	99.0	.1725	.0877	.1935	.2674	.1359	.2999
1.78	4	50	51.5	98.0	.1178	.0097	.1182	.3651	.0302	.3663
1.73	1	20	22.9	44.0	.2063	.1938	.2831	.6357	.5973	.8723
1.73	2	50	52.6	98.7	.1722	.1681	.2407	.2653	.2590	.3708
1.73	3	50	52.2	98.5	.1689	.0865	.1897	.2602	.1332	.2923
1.68	1	20	23.4	44.4	.2085	.1925	.2838	.6383	.5891	.8686
1.68	2	50	53.1	99.0	.1733	.1573	.2341	.2652	.2407	.3582
1.68	3	50	50.8	97.6	.1161	.0854	.1441	.3552	.2612	.4409
1.63	1	20	23.8	44.8	.2112	.1917	.2853	.6417	.5825	.8667
1.63	2	50	52.4	98.6	.1702	.1469	.2249	.2586	.2232	.3416
1.58	1	20	24.3	45.4	.2145	.1915	.2875	.6463	.5771	.8665
1.58	2	40	41.8	80.7	.1323	.1234	.1809	.3987	.3718	.5451
1.53	1	20	22.9	44.0	.1944	.1891	.2712	.5805	.5647	.8098

Table 7: Chosen values (continued) of  $t_p(\delta)$  and corresponding signal peaking times  $t_m(\delta)$  and  $t_m(\Delta)$ , and noise contributions in GeV jet scale and in mip.

## 5 Conclusion

Optimum values for the integration time for each readout channel of the hadronic end-cap calorimeter have been determined. A limited set of shaper times can be chosen (20, 30, 40 and 50 ns), one for each readout channel (other scenarios are also under study). Less than 3% excess total noise is found moving from the optimum  $t_p(\delta)$  values to these working values.

At the LHC luminosity of  $1.0 \times 10^{34} \text{ cm}^{-2}\text{s}^{-1}$  the signal to noise ratio for a mip will be in the range 0.14 to 1.3 for the first readout depth, 0.27 to 3.0 for the second readout depth, 1.7 to 3.4 for the third readout depth and 2.7 to 3.5 for the fourth readout depth.

We assume that the  $t_p(\delta)$  working range of the calorimeter can be adjusted according to the actual luminosity of the LHC by following the procedure of Cleland and Stern [5] where the effective working value of  $t_p(\delta)$  can be varied by weighting adjacent time bins for each readout channels.

Optimum  $t_p(\delta)$  need to be found in the case of jets. Correlations in pileup noise between readout channels forming a jet cluster will increase the pileup noise, perhaps requiring smaller optimum  $t_p(\delta)$ .

## References

- [1] H.Brettel et al., ATLAS - CAL - Note 61 (1994).
- [2] R.L. Chase, C. de La Taille, S. Rescia and N. Seguin, Nucl. Instr. and Meth., A330 (1993) 228-242.
- [3] T.Hodges et al., ATLAS - CAL- Note 60 (1994).
- [4] T. Sjöstrand CERN-TH. 7112/93.
- [5] B. Cleland and Stern, Nucl. Instr. and Meth., A338 (1994) 467.